

Tailoring Magnetism in Quantum Dots

Ramin M. Abolfath^{1,2}, Pawel Hawrylak², and Igor Žutić¹

¹*Department of Physics, State University of New York at Buffalo, Buffalo, New York 14260, USA*

²*Institute for Microstructural Sciences, National Research Council of Canada, Ottawa, K1A 0R6, Canada*

(Dated: March 23, 2022)

We study magnetism in magnetically doped quantum dots as a function of confining potential, particle numbers, temperature, and strength of Coulomb interactions. We explore possibility of tailoring magnetism by controlling the electron-electron Coulomb interaction, without changing the number of particles. The interplay of strong Coulomb interactions and quantum confinement leads to enhanced inhomogeneous magnetization which persist at higher temperatures than in the non-interacting case. The temperature of the onset of magnetization can be controlled by changing the number of particles as well as by modifying the quantum confinement and the strength of Coulomb interactions. We predict a series of electronic spin transitions which arise from the competition between the many-body gap and magnetic thermal fluctuations.

PACS numbers: 75.75.+a, 75.50.Pp, 85.75.-d

Magnetic doping of semiconductor quantum dots (QDs) provides an interesting interplay of interaction effects in confined geometries [1, 2, 3, 4, 5, 6, 7, 8] and potential spintronic applications [9]. In the bulk-like dilute magnetic semiconductors the carrier-mediated ferromagnetism can be photoinduced [10, 11] and electrically controlled by gate electrodes [12], suggesting possible nonvolatile devices with tunable optical, electrical, and magnetic properties [9]. QDs allow for a versatile control of the number of carriers, spin, and the effects of quantum confinement which could lead to improved optical, transport, and magnetic properties as compared to their bulk counterparts [1, 13, 14]. Unlike in the bulk structures, adding a single carrier in a magnetic QD can have important ramifications. An extra carrier can both strongly change the total carrier spin and the temperature of the onset of magnetization which we show can be further controlled by modifying the quantum confinement and the strength of Coulomb interactions.

We study the magnetic ordering of carrier spin and magnetic impurities in (II,Mn)VI QDs identified as a versatile system to demonstrate interplay of quantum confinement and magnetism [4, 5, 6, 15, 16, 17, 18]. Because Mn is isoelectronic with group-II elements it does not change the number of carriers which in QDs are controlled by either chemical doping or by external electrostatic potential applied to the metallic gates. The latter allows confinement of the carriers in a dot with tunable size and shape [2]. By using real space finite-temperature local spin density approximation (LSDA) [19] we study temperature (T) evolution of magnetic properties of QDs over a large parameter space. This approach allow us to consider QDs with varying number of interacting electrons (N) and Mn impurities (N_m) which already for small N and N_m becomes computationally inaccessible to the exact diagonalization techniques [18, 20]. We extend the previous studies of Coulomb interactions in magnetic QDs with $N_m = 1, 2$ at $T = 0$ [18] and $T > 0$ results us-

ing either Thomas-Fermi approximation or by applying Hund's rule with up to 6 carriers [17]. We reveal that the interplay of strong Coulomb interactions and quantum confinement leads to enhanced inhomogeneous magnetization which persist at higher temperatures than in the non-interacting case and the bulk structures [16, 17]. We refer to such a spin-polarized state in QD at zero applied magnetic field as "ferromagnetic" state [16, 17, 18].

Here we focus on magnetic QD in zero applied magnetic field described by the Hamiltonian $H = H_e + H_m + H_{ex}$, with the electron contribution $H_e = \sum_{i=1}^N [-\frac{\hbar^2}{2m^*} \nabla_i^2 + U_{QD}(\mathbf{r}_i)] + \frac{\gamma}{\epsilon} \sum_{i \neq j} \frac{e^2}{|\mathbf{r}_i - \mathbf{r}_j|}$, where \hbar is the Planck constant, m^* is the electron effective mass, and $U_{QD}(\mathbf{r})$ is the confining potential of a three-dimensional QD. The last term in the equation is the repulsive electron-electron (e-e) Coulomb interaction screened by the dielectric constant ϵ , $-e$ is electron charge, and γ accounts for reduction of Coulomb strength due to screening effects of the gate electrodes [21]. The Mn Hamiltonian is $H_m = \sum_{I,I'} J_{I,I'}^{AF} \vec{M}_I \cdot \vec{M}_{I'}$, where J^{AF} is the direct Mn-Mn antiferromagnetic coupling. The z -component of \vec{M}_I of impurity spin satisfies $M_z = -M, -M+1, \dots, M$, where we choose \hat{z} as the quantization axis and $M = 5/2$ for Mn. The electron-Mn (e-Mn) exchange Hamiltonian is $H_{ex} = -J_{sd} \sum_{i,I} \vec{s}_i \cdot \vec{M}_I \delta(\mathbf{r}_i - \mathbf{R}_I)$, where J_{sd} is the exchange coupling between electron spin \vec{s}_i , at $\mathbf{r}_i \equiv (\vec{\rho}_i, z_i)$, and impurity spin \vec{M}_I , at \mathbf{R}_I . An effective mean field Hamiltonian describing electrons can be obtained by replacing the Mn spins, that are randomly distributed, with a classical continuous field $H_e^{\text{eff}} = H_e - \sum_i J_{sd} n_m \frac{\sigma_i}{2} \langle M_z(\mathbf{r}_i) \rangle$, where n_m is the averaged density of Mn, and $\sigma = \pm 1$ for spin up (\uparrow), and down (\downarrow). The effective magnetic field seen by the electrons is the mean field induced by Mn. Assuming that impurities are in equilibrium with thermal bath it follows $\langle M_z(\mathbf{r}_i) \rangle = MB_M(Mb(\mathbf{r}_i)/k_B T)$ where $B_M(x)$ is the Brillouin function [22], k_B is the Boltzmann constant. Here $b(\mathbf{r}_i) = -Z_{Mn} J^{AF} \langle M_z(\mathbf{r}_i) \rangle + J_{sd} [n_{\uparrow}(\mathbf{r}_i) - n_{\downarrow}(\mathbf{r}_i)]/2$

is the effective field seen by the Mn [23]. The first term in $b(\mathbf{r}_i)$ describes the mean field of the direct Mn-Mn antiferromagnetic coupling [16]. Z_{Mn} is the averaged Mn coordination number, and $n_\sigma(\mathbf{r}_i)$ is spin-resolved electron density. We decompose the planar and perpendicular components of the confining potential of a single QD, and fit it to a realistic QD potential [24]. The resulting potential, U_{QD} , is a sum of a two-dimensional (2D) Gaussian $V_{QD} = V_0 \exp(-\rho^2/\Delta^2)$ and one-dimensional parabolic potential $V_{QD}^z = m^* \Omega^2 z^2/2$, where $\vec{\rho} \equiv (x, y)$. For V_{QD} we find that Gaussian potential is more realistic than usually studied parabolic potential. Here V_0 and Ω are the planar depth of the QD minimum, and the characteristic subband energy associated with the perpendicular confinement. In typical disk-shaped QDs, and low density of electrons, only the first subband is filled. After expanding the QD wave functions in terms of its planar $\psi_{i\sigma}(\vec{\rho})$ and subband wave function $\xi(z)$, we project H_e^{eff} into a two-dimensional Hamiltonian by integrating out $\xi(z)$. In LSDA the two-body Coulomb interaction can be written as sum of Hartree potential V_H and spin dependent exchange-correlation potential V_{XC}^σ . We use Vosko-Wilk-Nusair exchange-correlation functional [19], and express the Kohn-Sham Hamiltonian as

$$H_{KS} = \frac{-\hbar^2}{2m^*} \nabla_\rho^2 + V_{QD} + \gamma V_H + \gamma V_{XC}^\sigma - \frac{\sigma}{2} h_{sd}(\vec{\rho}), \quad (1)$$

where

$$h_{sd}(\vec{\rho}) = J_{em} \int dz |\xi(z)|^2 B_M \left(\frac{M b(\vec{\rho}, z)}{k_B T} \right), \quad (2)$$

and $J_{em} = J_{sd} n_m M$ is the e-Mn exchange coupling. The Kohn-Sham eigenvectors and eigenvalues of Eq. (1), $\psi_{n\sigma}(\vec{\rho})$, and $\epsilon_{n\sigma}$ are calculated numerically.

We illustrate our findings and the iterative solutions of Eq. (1) for (Cd,Mn)Te QD. The material parameters are $J_{sd} = 0.015$ eV nm³, $m^* = 0.106$, $\epsilon = 10.6$ [18], and we choose $Z_{Mn} J^{AF} = 0.02$ meV. The planar (x, y) , and perpendicular (z) , dimensions of the QD are taken as 42 nm and 1 nm with $n_m = 0, 0.025, 0.1$ nm⁻³. In the central region of QD of area $4a_B^{*2}$, where $a_B^* = 5.29$ nm is the effective Bohr radius in CdTe, $n_m = 0.1$ nm⁻³ corresponds to ≈ 10 Mn atoms. For a planar confinement, V_{QD} , we consider a Gaussian potential with $V_0 = -128$ meV, and $\Delta = 38.4$ meV, corresponding to $\omega_0 = 27$ meV. Here ω_0 is calculated by expanding V_{QD} in the vicinity of the minimum which yields $V_{QD} = V_0 + m^* \omega_0^2 \rho^2/2 + \dots$, with the strength $\omega_0 = \sqrt{2|V_0|/m^*}/\Delta$.

In QDs electron density is inhomogeneous, implying that both the electron spin density, $n_\uparrow(\vec{\rho}) - n_\downarrow(\vec{\rho})$, and Mn-magnetization density $\langle M_z(\vec{\rho}) \rangle \equiv M h_{sd}(\vec{\rho})/J_{em}$ are inhomogeneous. For $N = 8$ and $n_m = 0.1$ nm⁻³, we show the self-consistent spin density in Fig. 1(a), and Mn-magnetization density in Fig. 1(b). Outside the QD, $n_\sigma(\vec{\rho})$ decays exponentially, and an effective field $b(\vec{\rho})$

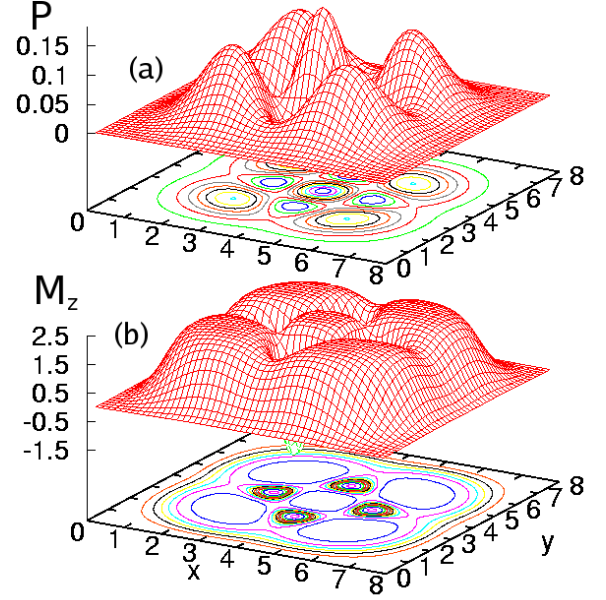


FIG. 1: The spatial density profile of electron spin density (a) and Mn-magnetization (b) for QD with $N = 8$ at $T = 1K$. Coordinates (x, y) are expressed in effective Bohr radius.

seen by Mn becomes negligible. This is consistent with vanishing $\langle M_z(\vec{\rho}) \rangle$ at the QD boundary [Fig. 1(b)].

We next turn to spatially-averaged quantities such as Mn-magnetization per unit area A , $\langle M_z \rangle = \frac{1}{A} \int d^2\rho \langle M_z(\vec{\rho}) \rangle$, electron (spin) polarization $P = (N_\uparrow - N_\downarrow)/N$, and the z -component of the total spin of electrons, $s_z = (N_\uparrow - N_\downarrow)/2$. In Fig. 2 we show $\langle M_z \rangle$ as a function of N for $n_m = 0.025$ nm⁻³, and both non-interacting ($\gamma = 0$), and interacting ($\gamma = 1$) electrons. The magnetic behavior of QD can be described based on the interplay of the many-body spectrum (determined by the shell structure of the confining potential, and e-e Coulomb interaction) and the strength of e-Mn exchange coupling J_{em} . In the following we summarize the spin structure of the QD in the absence and presence of J_{em} with $\gamma = 0, 1$.

i) $J_{em} = 0$: The shell structure of the 2D Gaussian potential is shown in Fig. 2(a). The energy gap between s -, p -, and d -orbitals is characterized by ω_0 . In contrast to 2D parabolic potential [1, 2], d -shell levels are not completely degenerate, and therefore we focus on $N > 6$ states. Degenerate levels d_+ and d_- are separated by an energy gap (1.5 meV) from d_0 -level, where $\pm, 0$ refer to angular momentum $l_z = \pm 1, 0$. However, e-e interaction changes the structure of d -shell as it overturns the ordering of the d -orbitals, e.g., the Kohn-Sham energies of pair of degenerate d_+ , and d_- are below d_0 (with energy gap ≈ 1 meV). Because of d -shell overturning, $N = 10, 12$

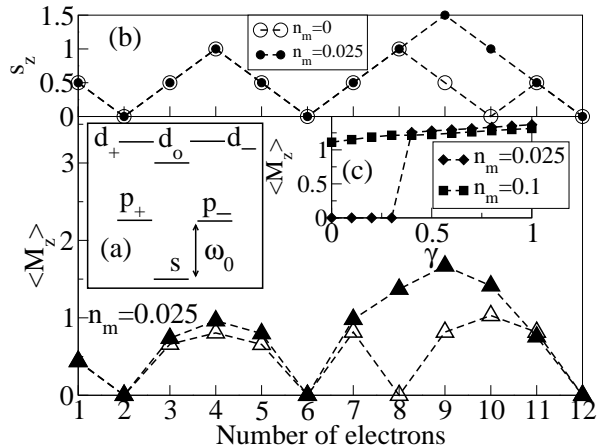


FIG. 2: The averaged magnetization per unit area $\langle M_z \rangle$ as a function of number of electrons N at $T = 1K$ and Mn-density $n_m = 0.025 \text{ nm}^{-3}$ for non-interacting ($\gamma = 0$, empty triangles) and interacting ($\gamma = 1$, filled triangles) electrons. The ground state of the QD switches between ferromagnetic and antiferromagnetic states as function of N . Coulomb interaction changes the state of $N = 8$ from antiferromagnetic to ferromagnetic state. (a) The schematic single particle levels of a 2D Gaussian confining potential. (b) The z -component of the total spin of electrons, s_z , as a function of N for $\gamma = 1$. (c) Antiferromagnetic-ferromagnetic transitions for $N = 8$ as function of n_m and γ .

form closed shells with $s_z = 0$, and $N = 7, 9, 11$ form open shells with $s_z = 1/2$. The $N = 8$ corresponds to half-filled shell with $s_z = 1$, and electron polarization, $P = 2/8$. The evolution of s_z as a function of N for $\gamma = 1$ is shown in Fig. 2(b) (empty circles).

ii) $J_{em} \neq 0$: $\gamma = 0$ and increasing e-Mn coupling to $J_{em} = 3.75 \text{ meV}$, leads to transitions $P = 0/8 \rightarrow 2/8$, and $P = 1/9 \rightarrow 3/9$ for $N = 8$, and 9, whereas $N = 10$ shows $P = 2/10$. For $\gamma = 1$, the dependence of P on J_{em} is negligible in s -, and p - shells. In contrast, in d -shell, we find transitions $P = 1/9 \rightarrow 3/9$, and $P = 0/10 \rightarrow 2/10$ for $N = 9$ and $N = 10$ at low T. However, we find no change in P for $N = 7, 8, 11$, and 12. Figure 2(b) (filled circles) show s_z as a function of N for $n_m = 0.025 \text{ nm}^{-3}$ ($J_{em} = 0.94 \text{ meV}$). Increasing the density of Mn to $n_m = 0.1 \text{ nm}^{-3}$ ($J_{em} = 3.75 \text{ meV}$) does not change s_z .

In Fig. 2, we observe that $\langle M_z \rangle = 0$ in closed shells ($N = 2, 6, 12$) for both $\gamma = 0$ and $\gamma = 1$, because of well separated s -, p -, and d - orbitals due to large $\omega_0 (\approx 30J_{em})$. Comparing $\langle M_z \rangle$ between $\gamma = 0$ and $\gamma = 1$ one can observe that the e-e interaction stabilizes the ferromagnetic state due to the spin Hund's rule. This condition is easily satisfied for open shells where the maximum electron polarization is obtained in half-filled shell with $N = 4$. The

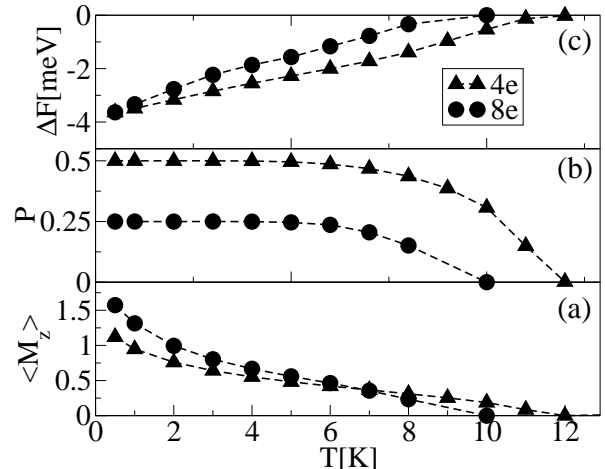


FIG. 3: Temperature evolution of Mn-magnetization per unit area $\langle M_z \rangle$ (a), the electron polarization P (b), and the free energy difference ΔF between ferromagnetic and antiferromagnetic QD (c) for $N = 4$ and $N = 8$. At low T, $N = 4, 8$ form half-filled shells with $P = 2/4, 2/8$. $T = T^*$, characterizes vanishing of $\langle M_z \rangle$, P , and ΔF .

$N = 8$ state (recall Fig. 1) is more interesting. At $\gamma = 0$ electrons fill single particle levels following the Pauli exclusion principle. Even with $J_{em} = 0.94 \text{ meV}$ (smaller than single particle e-h excitation gap), $N = 8$ forms closed shell and $P = \langle M_z \rangle = 0$. In the case of $\gamma = 1$, and because of d -shell overturning, polarized electrons in d_+ and d_- give $P = 2/8$, and finite $\langle M_z \rangle$. We also see that the maximum $\langle M_z \rangle$ occurs at $N = 9$ because $J_{em} = 0.94 \text{ meV}$ induces three polarized electrons in d -levels. Figure 2(c) reveals the dependence of magnetic transitions on γ , and n_m . With increasing $Z_{Mn}J^{AF}$, the transition to ferromagnetic state occurs at larger γ . Our findings clearly demonstrate that the magnetism induced by strong Coulomb interaction can be controlled by the electric gates or by changing the semiconductor host (and thus changing ϵ) without changing the number of carriers confined in QD. We also suggest that because of the sensitivity of the $\langle M_z \rangle$ to the electronic spin transitions, the former can be used to infer the spin of electrons, and could be potentially applied to manipulation of spin qubits in semiconductor nanostructures [9].

We next examine the temperature dependence of magnetism in QDs. In Fig. 3, we show $\langle M_z \rangle$ (a), P (b), and the free energy difference ΔF between ferromagnetic and antiferromagnetic states (c) for $N = 4$ and $N = 8$. The suppression of $\langle M_z \rangle$, shown in Fig. 3(a) is accompanied by a series of spin transitions in electronic states and sup-

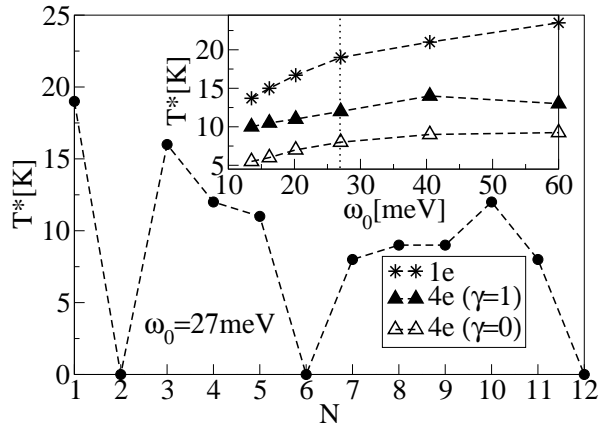


FIG. 4: T^* as a function of N for interacting electrons $\gamma = 1$, $\omega_0 = 27$ meV, and $V_0 = -125$ meV. Inset: The dependence of T^* on ω_0 for $N = 1$, $N = 4$ with $\gamma = 0$, and $\gamma = 1$. $\omega_0 = 27$ meV is marked as a dotted line. There is an optimal confining potential which maximizes T^* .

pression of P . At low T , the spin triplet is realized as the ground state of the $N = 4$, and $N = 8$ open p -, and d -shells (due to Hund's rule). We define a characteristic temperature, T^* , at which $\langle M_z \rangle = P = \Delta F = 0$.

In Fig. 4 we plot $T^*(N)$ for $\omega_0 = 27$ meV and $\gamma = 1$ which decreases non-monotonically with N . The inset shows $T^*(\omega_0)$ for $N = 1$, and $N = 4$ ($\gamma = 0, 1$). At low ω_0 , the e-e interaction strongly enhances T^* , while at large ω_0 the effect of confinement potential is dominant. Thus we find $T^*(\gamma = 1) \rightarrow T^*(\gamma = 0)$ with increasing ω_0 , which in turn gives rise to a peak in T^* . Several trends in calculated $T^*(N, \omega_0)$ can be obtained from a perturbative approach by approximating 2D Gaussian with 2D parabolic potential. Near $\langle M_z \rangle = P = 0$ for QD with one valence electron in s -, p -, or d -shells, we find $T^* = J_{em} \sqrt{\frac{M+1}{3n_m M}} [\int d^3 \mathbf{r} |\psi_f(\mathbf{r})|^4]^{1/2}$, where ψ_f is the wave-function of the highest occupied orbital, and $J^{AF} = 0$. For a given ω_0 , T^* decreases with N , e.g., $T_{N=3}^* = 0.7T_{N=1}^*$ and $T_{N=7}^* = 0.6T_{N=1}^*$. One can also show that $T^* \propto \sqrt{\omega_0}$, consistent with bound magnetic polarons [25].

In conclusion we have investigated the existence of magnetism in magnetically doped QDs, as function of particle numbers, confining potential, temperature and strength of Coulomb interactions, using finite-temperature LSDA. Our results show that QDs embedded in magnetic semiconductor host can be considered as ferromagnetic centers which exhibit spatial ordering in spin density and magnetization, even at elevated tem-

peratures where no such ordering exist in the host material [26]. In the limit of small ω_0 , where the Coulomb interaction among particles is the largest characteristic parameter of the QDs, we find magnetism substantially stronger than predicted from the non-interacting picture. In contrast to the carrier-controlled ferromagnetism in the bulk-like structures [10, 11, 12], we reveal that magnetism in QDs, can be tuned even at the fixed number of carriers by gate voltage which controls the inter-particle Coulomb interaction screening. For potential spintronic applications based on II-VI magnetic QDs, we anticipate that it is possible to further increase the magnetization and the temperature at which it vanishes. In addition to exploring a larger hole-Mn exchange coupling [22] in (II,Mn)VI QDs, it would also be advantageous to consider (II,Cr)VI QDs as there is a support for the room-temperature ferromagnetism in their bulk counterparts [27].

This work is supported by the US ONR, NSF-ECCS Career, the NRC HPC project, CIAR, and the CCR at SUNY Buffalo. We thank C. Dharma-wardana for stimulating discussions.

-
- [1] L. Jacak, P. Hawrylak, and A. Wojs, *Quantum Dots* (Springer, Berlin, 1998); D. Bimberg, M. Grundmann, N.N. Ledentsov, *Quantum Dot Heterostructures*, John Wiley & Sons (Chichester 1999).
 - [2] S. M. Reimann and M. Manninen, *Rev. Mod. Phys.* **74**, 1283 (2002), and the references therein.
 - [3] S. Tarucha, D. G. Austing, and T. Honda, R. J. van der Hage and L. P. Kouwenhoven, *Phys. Rev. Lett.* **77**, 3613 (1996).
 - [4] S. Mackowski, T. Gurung, T. A. Nguyen, H. E. Jackson, and L. M. Smith, G. Karczewski and J. Kossut, *Appl. Phys. Lett.* **84**, 3337 (2004).
 - [5] C. Gould, A. Slobodskyy, T. Slobodskyy, P. Grabs, D. Supp, P. Hawrylak, F. Qu, G. Schmidt, L.W. Molenkamp, *Phys. Rev. Lett.* **97**, 017202 (2006).
 - [6] Y. Léger, L. Besombes, J. Fernández-Rossier, L. Maingault, and H. Mariette, *Phys. Rev. Lett.* **97**, 107401 (2006); Y. Léger, L. Besombes, L. Maingault, D. Ferrand, and H. Mariette, *Phys. Rev. Lett.* **95**, 047403 (2005).
 - [7] R. M. Abolfath and P. Hawrylak, *Phys. Rev. Lett.* **97**, 186802 (2006).
 - [8] S. C. Erwin, Lijun Zu, Michael I. Haftel, Alexander L. Efros, Thomas A. Kennedy, David J. Norris, *Nature* **436**, 91 (2005).
 - [9] I. Žutić, J. Fabian, and S. Das Sarma, *Rev. Mod. Phys.* **76**, 323 (2004).
 - [10] S. Koshihara, A. Oiwa, M. Hirasawa, S. Katsumoto, Y. Iye, C. Urano, H. Takagi, and H. Munekata, *Phys. Rev. Lett.* **78**, 4617 (1997).
 - [11] Alvaro S. Nunez, J. Fernández-Rossier, M. Abolfath, and A. H. MacDonald, *J. Magn. Magn. Mater.* **272**, 1913 (2004).
 - [12] H. Ohno, D. Chiba, F. Matsukura, T. Omiya, E. Abe, T. Dietl, Y. Ohno, K. Ohtani, *Nature (London)* **408**, 944

- (2000); D. Chiba, M. Yamanouchi, F. Matsukura, and H. Ohno, *Science* **301**, 943 (2003).
- [13] M. Holub, S. Chakrabarti, S. Fathpour, and P. Bhattacharya, Y. Lei, and S. Ghosh, *Appl. Phys. Lett.* **85**, 973 (2004).
- [14] S. C. Erwin and I. Žutić, *Nature Mater.* **3**, 410 (2004).
- [15] P. Hawrylak, M. Grabowski and J.J. Quinn, *Phys. Rev. B* **44**, 13082 (1991).
- [16] J. Fernández-Rossier and L. Brey, *Phys. Rev. Lett.* **93**, 117201 (2004). J. Fernández-Rossier, *Phys. Rev. B* **73**, 045301 (2006).
- [17] A. O. Govorov *Phys. Rev. B* **72**, 075358 (2005); *Phys. Rev. B* **72**, 075359 (2005).
- [18] F. Qu and P. Hawrylak, *Phys. Rev. Lett.* **95**, 217206 (2005); *Phys. Rev. Lett.* **96**, 157201 (2006).
- [19] C. Dharma-wardana, and F. Perrot in *Density Functional Theory*, Edited by E. K. U. Gross, and R.M. Dreizler (Plenum Press, New York, 1995).
- [20] The size of the Hamiltonian matrix to be diagonalized for just 10 Mn (spin-5/2) is $6^{10} \approx 6 \times 10^7$.
- [21] N. A. Bruce and P. A. Maksym, *Phys. Rev. B* **61**, 4718 (2000).
- [22] J. K. Furdyna, *J. Appl. Phys.* **64**, R29 (1988).
- [23] S. Das Sarma, E. H. Hwang, and A. Kaminski, *Phys. Rev. B* **67**, 155201 (2003).
- [24] J. Kyriakidis, M. Pioro-Ladriere, M. Ciorga, A. S. Sachrajda, and P. Hawrylak, *Phys. Rev. B* **66**, 035320 (2002).
- [25] D. R. Schmidt, A. G. Petukhov, M. Foygel, J. P. Ibbetson, and S. J. Allen, *Phys. Rev. Lett.* **82**, 823 (1999).
- [26] T. Dietl, A. Haury and Y. Merle d'Aubigné, *Phys. Rev. B* **55**, R3347 (1997).
- [27] H. Saito, V. Zayets, S. Yamagata, and K. Ando, *Phys. Rev. Lett.* **90**, 207202 (2003).